

Large eddy simulation of a partially-confined triangular jet with self-excited low-frequency oscillation

M. Xu and J. Mi

State Key Laboratory of Turbulence & Complex Systems, College of Engineering
Peking University, Beijing 100871, China

Abstract

This paper reports large eddy simulation (LES) of a self-excited oscillating jet issuing initially from a small triangular orifice into a circular chamber. The case simulated is that measured experimentally by England et al. (*Expts. Fluids* **48**, 2010, pp. 69-80). Present calculations agree well with previous measurements.

It is found that a jet from the triangular orifice discharges into the chamber, re-attaches the inner wall and oscillates roughly gyroscopically about the chamber axis. In the mean sense, the jet exhibits axis-switching in its cross-section and rotates by 180° over a downstream distance of $x = 0.5D$ (chamber diameter). Importantly, three strong longitudinal vortices occur in conjunction with the exit triangle sides, interacting with the central jet and also surroundings, at $x/D \leq 1$. These three vortices appear to merge as a larger one around the location where the unmixed core region is ended. Evidently as well, some ambient fluid outside is induced into the chamber and dashes upstream together with the reversed jet fluid, forming a secondary surrounding flow swirling in the opposite sense to the oscillation.

Introduction

A small flow ejecting into a relatively large specific chamber can produce large-scale low-frequency oscillations — this flow is complex and termed as a self-excited oscillating jet. Compared with simple, non-oscillation, free jets, e.g. round or triangular jets, the self-excited oscillating jet produces greater spreading rate, higher velocity decay rate and larger-scale velocity fluctuations which are all a source of large-scale turbulent mixing [1-5]. Such flows may be used to improve the performance of industrial burners, multi media mixers and reactors in the processing industry. For example, the self-excited precessing jet (PJ) devices [1] and new generation oscillating-jet devices [2] have been beneficially installed at cement, glass and lime kilns.

In early studies with a circular orifice, Nathan et al. [3] showed that, for the PJ to oscillate reliably, the chamber inlet-expansion ratio must be larger than about 5.0, i.e. $D/d_{e1} > 5$ (see Fig. 1 for notations), and the length ratio of the chamber must be in the range of $2.6 \leq L/D \leq 2.8$. A small lip of height $h_2 = (D - d_2)/2 \leq 0.1D$ is usually attached to the chamber exit. Measurements and observations of the PJ flow [4, 5] show that the Strouhal number of the precession has a significant influence on the oscillating mixing field, while the Reynolds number does not.

Mi et al. [2] then found that the non-circular orifice can enhance the oscillation process, relative to the circular inlet case. In particular, the use of the triangular inlet is one of the best options for this enhancement. In a parametric study of the oscillating triangular jet (OTJ) nozzle, Lee et al. [6, 7] found that the spreading angle of the OTJ flow from the nozzle is significantly smaller than that of the PJ flow and it varies more gradually over

broad ranges of the ratios L/D and D/d_{e1} . A designer therefore has the flexibility not only to accommodate a much lower supply pressure but also to choose the jet spreading angle. England et al [8] investigated the effect of the density ratio of the OTJ fluid to ambient fluid on the resulting OTJ flow downstream from the nozzle. The initial spread and decay of the emerging jet were found to depend upon the density ratio while the dominant oscillation frequency decreases with increasing the density ratio.

However, the OTJ flow is highly unsteady and complex, and so the detailed information on the instantaneous flow structure inside the chamber is still lacking. This makes it difficult to understand the formation mechanism of the oscillation. The present work is part of the study that aims to eventually address this deficit. We use Large Eddy Simulation (LES) to visualize the OTJ flow structure. Note that the LES can provide the quantitative detail of the whole flow, which remains impossible by experiments. To our best knowledge, it is the first time to study the OTJ flow by LES.

Following the experimental investigation by England et al. [8] on the OTJ flow, the present study is aimed at examining both the mean and instantaneous OTJ flow structures mainly inside the chamber under the same initial and boundary conditions. The simulation was performed for the same Reynolds number as used in [8], i.e., $Re_1 = 17,900$, where $Re_1 \equiv U_1 d_{e1}/\nu$ with U_1 being the mass-averaged velocity at the orifice-inlet, d_{e1} the orifice equivalent diameter and ν the kinematic viscosity of the fluid.

Computational details

The filtered governing equations of an unsteady incompressible viscous flow for LES are

$$\frac{\partial \bar{u}_i}{\partial t} + \frac{\partial \bar{u}_i \bar{u}_j}{\partial x_j} = -\frac{\partial \bar{p}}{\partial x_i} + \frac{1}{Re_1} \frac{\partial^2 \bar{u}_i}{\partial x_j \partial x_j} - \frac{\partial \tau_{ij}}{\partial x_j} \quad (1)$$

$$\frac{\partial \bar{u}_i}{\partial x_i} = 0 \quad (2)$$

where x_i ($i = 1, 2, 3$) are the coordinates, as replaced later by (x, y, z) , \bar{u}_i are the corresponding filtered velocity components and \bar{p} is the filtered pressure. The subgrid-scale (SGS) stress tensor τ_{ij} , defined by

$$\tau_{ij} = \overline{u_i u_j} - \bar{u}_i \bar{u}_j \quad (3)$$

is modeled using the model by Germano et al. [9], together with the least-square method suggested by Lilly [10].

A finite-volume method based on integration over the control volume was used to solve the model equations (1) and (2). The bounded central difference scheme was used for spatial

discretizations, and the second-order three-level implicit scheme was used for time advancement. The SIMPLEC method was used for the pressure-velocity coupling.

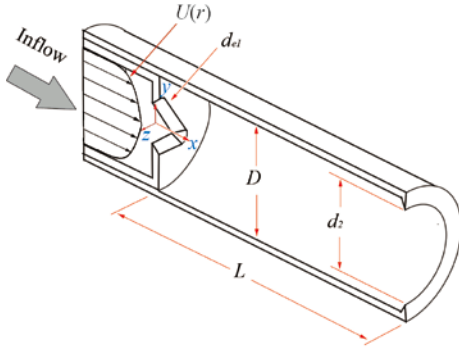


Fig. 1: A schematic diagram of the OTJ nozzle showing notation

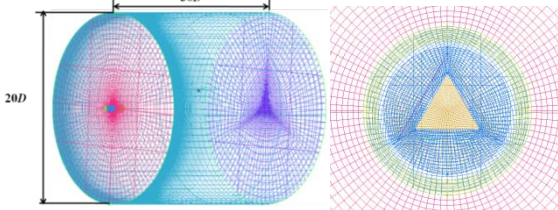


Fig. 2: Grid distribution of calculation for the OTJ flow. (a) 3D view of the computational domain; (b) zoom of the grid around the symmetry axis in a plane $x = \text{constant}$.

Figure 1 shows the schematic diagram of the OTJ nozzle used in present study and also by England et al. [8]. The OTJ flow is partially inside a circular chamber of diameter $D = 26.5\text{mm}$ and length $L = 2.5D$ with an equally-triangular inlet of equivalent diameter $d_{e1} = D/3.5$ and chamber exit diameter $d_2 = 0.82D$. The OTJ nozzle is connected to a smooth straight pipe of internal diameter $D_0 = 0.75D$, and length $L_0 = 2D$. Here x, y, z denote the streamwise, spanwise and lateral directions, respectively. The origin of the coordinate locates at the inlet triangular center.

At the inlet ($x = -L_0$) the velocity profile of a fully developed turbulent pipe flow was given, which was similar to that of England et al. [8]. The velocity profile was determined by the empirical $1/7^{\text{th}}$ power-law, i.e.,

$$U(r)/U_c = (1-2|r|/D_0)^{1/7} \quad (4)$$

where U_c is the centerline velocity and $U(r)$ is the streamwise component of time-averaged velocity at radial distance, $r \equiv (y^2+z^2)^{1/2}$, from the centerline of the pipe. At the pipe-inlet and the triangular orifice the bulk mean velocities $U_j = 4.8\text{m/s}$ and $U_1 = 33.3\text{m/s}$, respectively. In most experimental set-ups, there are background disturbances present in the jet produced. In the present study, we constructed the background disturbance such that its frequency spectrum consists of the Kolmogorov spectrum in the inertial region and the Pao spectrum in the dissipation region, respectively [11]. The background disturbance was randomly distributed in space at the jet inlet, and the amplitude (r.m.s. value) of the background disturbance was set to be $u_j = 0.01U_j$. No-slip boundary condition is applied at the nozzle surface. At the radial far-field boundary, a free-slip boundary condition is applied and a zero-gradient (Neumann) condition is imposed on both of the inlet ($x=0$) and outlet ($x=L$) sides.

The computational domain included the complete internal chamber and some external space of the nozzle, see Fig. 2a. The external region downstream from the chamber exit provided the needed ‘buffer’ region that was found important for the external near-field behavior of jet flows by Babu and Mahesh [12]. The downstream and side far-field boundaries of the

computational domain were located at $30D$ downstream of the chamber inlet exit and $10D$ from the nozzle axis, respectively. A structured non-uniform grid arrangement was employed, see Fig. 2. The computational grid consisted of about 2 million cells with $160(x) \times 112(y) \times 112(z)$ grid points. The grid was clustered near the inner boundaries of the chamber to capture the high shear in that region. The grid resolution was checked by performing a simulation at a higher resolution of $256(x) \times 128(y) \times 128(z)$ grid points. The difference in the oscillation frequency was less than 2%, which confirmed the mesh independence of the solution.

The time step independence of the solutions was tested, and the time step used was 0.00005s , which was chosen as the upmost value on the balance of convergence and CPU time. The simulations were run for a time period of 60 cycles of the oscillation before a statistically steady state was reached and mean values were collected. The computations in this paper were carried out on a HP Z800 workstation with 16 CPUs.

Results and discussion

Characteristics of the mean OTJ flow

To examine the mean OTJ flow, contours of the streamwise mean velocity calculated from the central xy -plane are shown in Fig. 3 whereas those from six different cross-sections of $x/D = 0.1 \sim 2.5$ inside the chamber are displayed in Figs. 4(a-f), together with cross-sectional views of the mean streamlines. Note that the contours and streamlines were obtained by averaging the instantaneous data over a time period of 60 cycles of the global oscillation. Fig. 3 demonstrates that the mean velocity of the central flow at $x/d_{e1} \leq 3.5$ is generally higher than the average inlet velocity U_1 ; also, the exit velocity takes the maximum at the mid-way between the nozzle edge and jet center (see Fig. 4a-b). These observations are expected because the upstream orifice nozzle should produce such a distribution of the exit velocity that is relatively high in the central region and reaches the maximum somewhere between the exit center and edge [13]. As expected, too, the mean OTJ flow in the xy plane is asymmetric, see Fig. 3, due to the orientation of the triangular exit.

Fig. 4(a) demonstrates that, immediately downstream from the inlet, at $x/D = 0.1$, the intensely-spaced contours of the mean velocity $\geq 0.4U_1$ well follow the exit triangular shape. As x increases, the OTJ flow evolves significantly: the jet cross-section appears to ‘rotate’ by 180° over a distance of $x/D = 0.5$, exhibiting the ‘axis-switching’ phenomenon, which is often referred to by investigators of noncircular jets (e.g., Gutmark and Grinstein [14]; Mi et al. [15]). It is also revealed by the streamlines that there is a secondary flow going anti-clockwise around the central jet inside the chamber at $x/D \leq 1$. This secondary swirling flow is very strong at $x/D \leq 0.3$. Furthermore, there exist three streamwise vortices, all rotating anti-clockwise, at each side of the exit ‘triangle’. These vortical structures exist at least between $x/D = 0.1$ and $x/D = 0.5$. As the flow proceeds downstream, they entrain and mix with the surrounding fluid, thus becoming larger in size; concurrently, their strength of rotation weakens. Quite evidently as well, these longitudinal structures move along with the cross-sectional ‘rotating triangle’ sides. These three vortices appear to merge as one larger vortex approximately at $x/D = 1$ or $x/d_{e1} = 3.5$, around which the unmixed core region is ended. For $x/D \geq 2$, see Figs. 4(e-f), the ‘memory’ of the initial triangular shape of the OTJ is completely lost. The streamlines show that, in the mean sense, the fluid from the main jet spreads out with some tendency to rotate at $x/D = 2$. Just at the chamber outlet, i.e., $x/D = 2.5$, as demonstrated by the streamlines, some ambient fluid from the outside is induced into the chamber. In addition, Figs. 3 and 4(a-f) indicate that the in-

chamber flow may be characterized as the central forward flow and outer low-speed backward flow which occupies most of the inner space at $x/D \leq 1.25$. Perhaps noteworthy, some low-speed forward flow exists in a small space near the inner wall at $x/D \leq 0.5$.

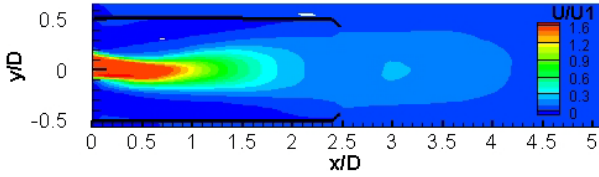


Fig. 3: Contours of the streamwise mean velocity in the central xy -plane

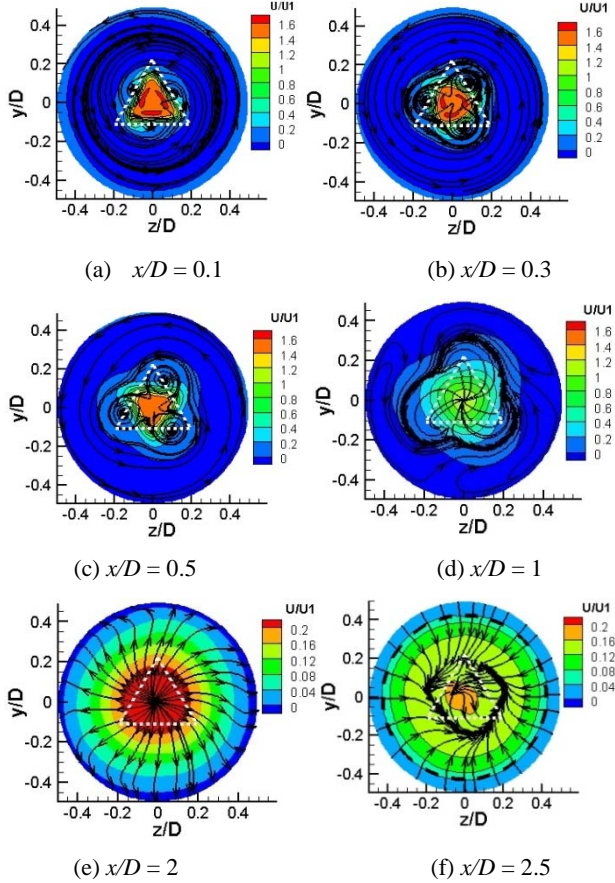


Fig. 4: Cross-sectional views of longitudinal mean velocity contours and streamlines at different x/D .

To verify the present simulation by experiment, we plot in Figs. 5(a-b) the inverse centerline velocity decay (U_1/U_c) and streamwise variation of the half-velocity widths ($y_{1/2}$, $z_{1/2}$) together with previous PIV measurements of England et al. [8] in the similar OTJ flows outside the chamber. Here U_c denotes the centerline mean velocity, while the half-velocity widths $y_{1/2}$ and $z_{1/2}$ represent the lateral locations at which the mean velocity is $U = 0.5U_c$. As demonstrated, the LES results agree reasonably well with those of England et al [8] measured over the range $2.9 \leq x/D \leq 5.1$. Fig. 5(a) shows that U_c decreases monotonically in the chamber ($x/D < 2.5$), then increases at $x/D < 3$ immediately downstream of the chamber exit, and decreases again farther downstream at $x/D > 3$. The increase over the near-field region $2.5 < x/D < 3$ can be explained here. At the exit plane of the chamber, a circular lip of diameter $d_2 = 0.82D$ is placed with a backward-facing 45° ramp. The asymmetric jet emerging from the chamber therefore would be deflected at 45° by the lip so that it passes across the nozzle axis in the near-field (centred at $0.5D$

downstream of the exit or $x/D = 3$) almost all the time, resulting in the centerline mean velocity being relatively higher at $x/D < 3$.

Fig. 5(b) shows the half-velocity widths ($y_{1/2}$, $z_{1/2}$) of the OTJ in the central xy and xz planes. These widths were calculated from y -direction and z -direction across the entire jet at several x/D values and at each location the average values of $y_{1/2}$ and $z_{1/2}$ on either side of the jet centerline are accounted. As expected, both $y_{1/2}$ and $z_{1/2}$ increase monotonically with downstream distance. However, the growth of $y_{1/2}$ is faster than that of $z_{1/2}$ for $x/D > 5$. This is likely because the oscillating triangular jet has preferred azimuthal directions at the three corners, e.g., one in the xy plane, as observed by Lee et al. [7]. Note that the jet flow precesses (i.e. rotates azimuthally) about the chamber axis in a continuously unstable manner.

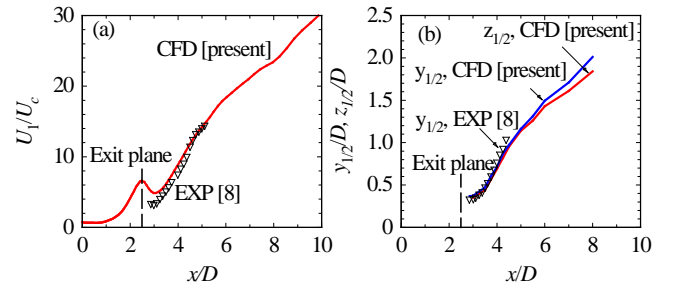


Fig. 5: (a) Mean velocity decay along the centerline of the OTJ flow and (b) streamwise variations of half-velocity widths $y_{1/2}$ and $z_{1/2}$.

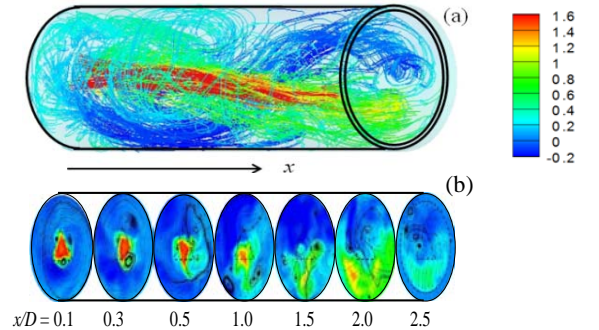


Fig. 6: Typical instantaneous OTJ flow structure inside the chamber. Part (a): 3-D views of streamlines; part (b): projections of streamlines and longitudinal velocity contours in the yz planes located at different x/D indicated.

Characteristics of the instantaneous OTJ flow

The typical instantaneous OTJ flow structure inside the chamber is illustrated by three-dimensional (3-D) streamlines in Fig. 6 and also by the longitudinal projections of streamlines in Fig. 7. It is demonstrated clearly that the jet issuing from the triangular exit suddenly expands into the chamber, re-attaches the inner wall and oscillates roughly gyroscopically about the chamber axis due to some natural instabilities. Notably, three streamwise vortices are initially formed in conjunction with the exit triangle sides, interacting with each other and also with the central main jet. Simultaneously a quantity of ambient fluid is induced into the chamber from the outside and goes upstream together with the reverse fluid from the jet itself, forming a secondary flow rotating around in the opposite sense to the oscillation. These flow characteristics are qualitatively consistent with experiments by deduction [6]. Unfortunately, however, the latter cannot display any similar 3-D pictures inside a chamber due to the complexity of the OTJ flow and also the constraint of those optical measurement technologies.

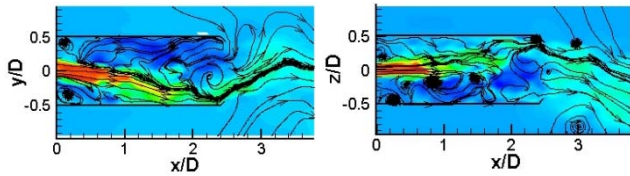


Fig. 7: Longitudinal projections of streamlines and streamwise velocity contours in the xy plane (a) and the xz plane (b).

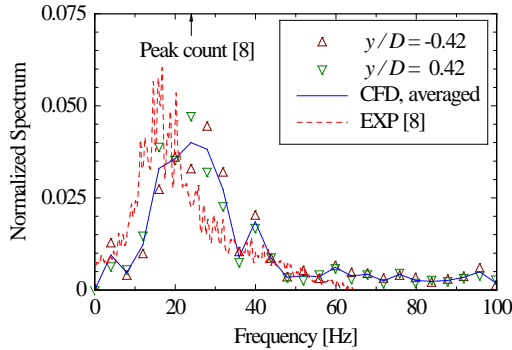


Fig. 8: Frequency spectra of velocity at $x/D = 2.49$, $y/D = \pm 0.42$ and $z/D = 0$.

In order to obtain the average oscillation frequency precisely, the frequency spectra of the fluctuating velocity at $x/D = 2.49$, $y/D = \pm 0.42$ and $z/D = 0$ is shown in Fig. 8. The pressure spectrum measured by England et al. [8] at $x/D = 2.49$, $y/D = 0.42$ and $z/D = 0$ is also included for comparison. Obviously, all the spectra exhibit a broad peak. If we choose the frequency at which the spectrum is the highest as the dominant oscillation frequency f_p , the present LES data show that $f_p \approx 24\text{Hz}$. This value of the frequency agrees well with that obtained by England et al. with the *peak count* method but is higher than that determined from their spectrum. The corresponding Strouhal number defined by $St \equiv f_p d_{ei}/U_1$ is approximately 0.0054. This St value is about two orders of magnitude lower than that of acoustically forced flow from a circular duct ($0.15 \leq St \leq 0.6$) [16] and a triangular duct ($St \approx 0.3$ and 0.51) [17].

Conclusion

In the present study, we have simulated using LES the oscillating triangular jet (OTJ) produced through a specific chamber described in Fig. 1 and Section 2. Calculations of the mean OTJ flow at $Re_1 = 17,900$ are well verified by recent measurements of England et al. [8]. The simulated OTJ flow displays several interesting aspects that are summarised below:

- (1) After discharging downstream into the chamber, the jet re-attaches the inner wall and oscillates about the chamber axis only roughly in a gyroscopic fashion.
- (2) The axis-switching phenomenon, often occurring in non-circular free jets [14], also takes place in this partially-confined and oscillating triangular jet.
- (3) Three strong longitudinal vortices arise along with the jet in the initial region at $x/D \leq 1$. These three vortices appear to merge as a larger one or disappear near the location where the unmixed core region is ended. The swirling intensity is expected to increase upstream and achieves the maximum near the chamber upstream end.
- (4) Due to the jet entrainment inside the chamber, some external fluid is induced into the chamber and joins the reverse fluid from the jet to form a secondary swirling flow, which occupies most of the chamber.

- (5) The in-chamber flow may be overall characterized to be the central forward OTJ flow and the outer backward swirling stream which occupies most of the inner space at $x/D \leq 1.25$.

Acknowledgment

The support of Nature Science Foundation of China through Grant#10772006 for the work is gratefully acknowledged. Mr. Pengfei Li provided a great help for the simulations.

Reference

- [1] Luxton R. E. & Nathan G. J., (1987): Patent Application No PI4068/87, Australian Patent Office.
- [2] Mi J., Nathan G. J. & Luxton R. E., "Family of Oscillating Jets". Pat App No. PCT/ AU98/00959 (Granted worldwide).
- [3] Nathan G., Hill S. & Luxton R., An axisymmetric 'fluidic' nozzle to generate jet precession, *J. Fluid Mech.*, **370**, 1998, 347-380.
- [4] Mi J. & Nathan G. J., Self-excited jet-precession Strouhal number and its influence on downstream mixing field, *J. Fluids Struct.*, **19**, 2004, 851-862.
- [5] Mi J., Nathan G. J. & Wong C. Y., The influence of inlet flow condition on the frequency of self-excited jet precession, *J. Fluids Struct.*, **22**, 2006, 129-133.
- [6] Lee S. K., Study of a naturally oscillating triangular-jet flow. PhD thesis, School of Mechanical Engineering, The University of Adelaide, Australia. 2009. <http://hdl.handle.net/2440/58581>
- [7] Lee S. *et al.*, Low kinetic-energy loss oscillating-triangular-jet nozzles, *Exp. Therm. Fluid Sci.*, **27**, 2003, 553-561.
- [8] England G. *et al.*, The effect of density ratio on the near field of a naturally occurring oscillating jet, *Expt. Fluids*, **48**, 2010, 69-80.
- [9] Germano M. *et al.*, A dynamic subgrid - scale eddy viscosity model, *Phys. Fluids A: Fluid Dynamics*, **3**, 1991, 1760.
- [10] Lilly D., A proposed modification of the Germano subgrid - scale closure method, *Phys. Fluids A: Fluid Dynamics*, **4**, 1992, 633.
- [11] Pope S., *Turbulent flows* Cambridge Univ. Press, 2000.
- [12] Babu P. & Mahesh K., Upstream entrainment in numerical simulations of spatially evolving round jets, *Phys. Fluids*, **16**, 2004, 3699.
- [13] Mi J., Nobes D. S. & Nathan G. J., Influence of jet exit conditions on the passive scalar field of an axisymmetric free jet, *J. Fluid Mech.*, **432**, 2001, 91-125.
- [14] Gutmark E. & Grinstein F., Flow control with noncircular jets, *Annu. Rev. Fluid Mech.*, **31**, 1999, 239-272.
- [15] Mi J., Kalt P. & Nathan G., On Turbulent Jets Issuing from Notched-Rectangular and Circular Orifice Plates, *Flow, Turbulence and Combustion*, **84**, 2010, 565-582.
- [16] Crow S. & Champagne F., Orderly structure in jet turbulence, *J. Fluid Mech.*, **48**, 1971, 547-591.
- [17] Schadow K. *et al.*, Selective control of flow coherence in triangular jets, *Expt. Fluids*, **6**, 2004, 129-135.